# Performance of Trellis Coded Modulation Schemes on Shadowed Mobile Satellite Communication Channels

Chinthananda Tellambura, Qiang Wang, and Vijay K. Bhargava, *Fellow, IEEE*

***Abstract*—The Canadian mobile satellite (MSAT) channel has been modeled as the sum of lognormal and Rayleigh components to represent foliage attenuation and multipath fading, respectively. Several authors have applied trellis coded modulation (TCM) schemes to this channel, estimating the bit error performance via computer simulation. In this paper, analytical expressions are derived for the pairwise error probability (PEP) of TCM schemes over this channel under ideal interleaving. The analysis is applied to three detection strategies: ideal coherent detection, pilot-tone aided detection, and differential detection. The results are substantiated by means of computer simulation. In addition, first-order statistics of absolute and differential phases of a shadowed Rician process are examined.**

## I. List of Principal Symbols

| | |
|---|---|
| $\alpha_k$ | Complex channel gain for the $k$th symbol interval. |
| $\hat{\alpha}_k$ | Channel gain estimate for the $k$th symbol interval. |
| $b_0$ | Variance of channel gain. |
| $b_1$ | Variance of channel gain estimate. |
| $\gamma_s$ | Average signal energy-to-noise spectral density ratio. |
| $\boldsymbol{x}$ | Transmitted codeword. |
| $\hat{\boldsymbol{x}}$ | Erroneous codeword. |
| $f_d$ | Maximum Doppler frequency. |
| $\mu$ | Correlation coefficient between $\alpha_k$ and $\hat{\alpha}_k$. |
| $P_b$ | Average bit error probability. |
| $T_s$ | Channel symbol interval. |

## II. Introduction

To improve the performance of mobile communication systems (e.g., mobile satellite and cellular mobile systems), several authors have considered the application of TCM schemes to such channels. In particular, Divsalar and Simon [1], [2] have presented a rather complete analysis of TCM for the ideally interleaved Rician fading channel when coherent or differentially coherent detection methods are used. Their analysis includes derivation of a Chernoff upper bound on the pairwise error probability. In this case, the Chernoff bound not only yields a union upper bound on the average bit error probability of TCM operating on the Rician fading channel, but also provides the primary criteria for designing the optimal TCM for the fading channel [3].

Manuscript received February 1, 1993; revised April 30, 1993.

The authors are with the Department of Electrical and Computer Engineering, University of Victoria, Victoria, B.C., Canada V8W 3P6.

IEEE Log Number 9214310.

Typically, mobile satellite channels are modeled as Rician; that is, the received signal consists of a *constant* line of sight (LOS) signal component and a Rayleigh distributed diffuse signal component. In contrast, to account for the effect of foliage attenuation or blocking in a shadowed channel, the LOS component is assumed to be distributed as a lognormal variate. In application to the Canadian MSAT program, this model has been presented by Loo [4]–[7] and has been found to agree with measured data. A lower angle of elevation ($15°$–$20°$) between a mobile user and a geosynchronous satellite implies that the effect of shadowing is more pronounced in Canada than in the United States [8]. We describe this model in more detail later.

Many studies have been carried out to determine the applicability of TCM to this channel model; some of them include [8]–[12]. McLane *et al.* in [8], [9] have evaluated the performance 8-PSK and 8-DPSK trellis codes over the fast fading shadowed Rician channel via computer simulation. In his thesis work, Lee [10] has presented a comprehensive study of *light*[1] and *average* shadowed Rician models, including a chapter on the performance of TCM over such channels. The use of a convolutional interleaver in conjunction with several TCM schemes over the same channel has been presented by Lee and McLane [11]. Again, these two papers rely on computer simulation. The performance of TCM with coherent detection over the shadowed Rician fading channel has been presented by McKay *et al.*, where the Chernoff bound on the PEP is computed with the aid of numerical integration [12]. Another related paper [13] has described computer models of the common fading channels based on underlying Gaussian processes.

To date, the only analytical expressions available for this case have been presented by Huang and Campbell [14], and their results are limited to differentially coherent detection and the *slow* fading, shadowed Rician channel. Thus, unlike the case of Rician fading channels, an analytical basis for evaluating the performance of TCM over the shadowed Rician channel is missing. This paper attempts to fill the gap by providing new, analytical error bounds for TCM schemes over both slow and fast fading, shadowed Rician channels. The error bounds are derived for three detection schemes: ideal coherent detection, coherently differential detection, and pilot-tone based detection. Our pairwise error probability bounds

[1] The terms light and average denote the degree of fading, and the heavy fading channel is not considered here.

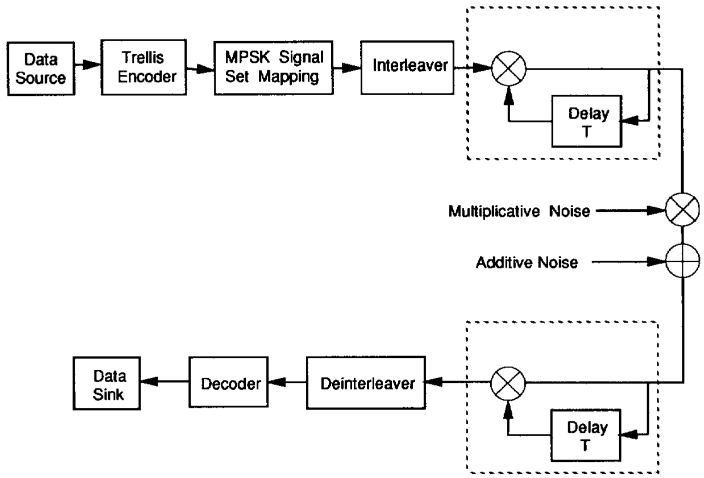


Fig. 1. Baseband system model where $T_s$ is the symbol period.

resemble those of the Rician channel, and as such can be used for both evaluating the bit error performance and for finding optimal codes for such channels.

In [15], the authors derive the approximate PEP of both TC-MPSK (trellis coded $M$-ary phase shift keying) and TC-MDPSK (trellis-coded $M$-ary differential phase shift keying) over Rician ideally interleaved channels. Our approximation was based on the saddle point method [16], [17], and the accuracy of this approximation was confirmed by extensive numerical comparisons. In this paper, we extend this earlier result to the shadowed Rician fading channel. The accuracy of these new bounds is confirmed by Monte-Carlo simulation results. We also derive the approximate probability density functions (pdf's) of both the absolute and differential phases, and show that the absolute phase is Gaussian for small values.

The paper is organized as follows. Section II describes the system model used here and the characterization of the shadowed Rician model. The approximate PEP of TC-MPSK and TC-MDPSK is derived in Sections III and IV. First order statistics of the phase of a shadowed channel are examined in Section V. Simulation results are presented in Section VI. Finally, conclusions are provided in Section VII.

## III. System and Channel Model

We consider a typical system model [1] as shown in Fig. 1. Binary input data is convolutionally encoded at rate $n/(n+1)$. The encoded $n+1$ bit words are block interleaved and mapped into a sequence $\boldsymbol{x} = (\hat{x}_1, \hat{x}_2, \cdots, \hat{x}_N)$ of $M$-ary PSK symbols, which constitute a normalized constellation, that is, $|x_k|^2 = 1$ for all symbols. For TC-MDPSK, additional differential encoding/decoding is done as shown in Fig. 1. The receiver deinterleaves and then applies soft-decision Viterbi decoding.

In this work, we only consider *ideally interleaved* channels. The ensuing independent fading approximation allows us to obtain a simple upper bound on the average bit error probability, which gives the performance limits of practical systems. In fact, the ideal interleaving condition can be achieved without much difficulty for some mobile communication systems. For instance, typical Doppler spread and the symbol duration product varies in the range $0.01 \leq f_d T_s \leq 0.1$ for $L$-band frequencies, at 2400 baud rate and at normal vehicle speeds. The use of interleaving for this application has been studied by several authors, and it is found that total interleaving delay requirements can be met by several methods [8].

Since we assume that the interleaving depth is sufficient to make channel fading appear independent from one symbol interval to another, we ignore the scrambling of the encoder output sequence by the interleaver. Thus, the transmitted signal is represented in the baseband as [18]

$$e(t) = \sum_{k=-\infty}^{\infty} v_k s(t - kT_s) \tag{1}$$

where $s(t)$ is a unit-energy pulse such that it satisfies Nyquist's conditions for zero inter-symbol interference after the receiving filter, and

$$v_k = \begin{cases} x_k & \text{TC-MPSK} \\ v_{k-1} x_k & \text{TC-MDPSK,} \end{cases} \tag{2}$$

where $x_k$ denotes the $k$th convolutional encoder output. The receiver employs a filter matched to $s(t)$. Therefore, the received sample corresponding to the $k$th coded symbol can be denoted by

$$y_k = \alpha_k v_k + n_k \tag{3}$$

where $n_k$ is a complex-Gaussian random variable with zero mean and variance $\sigma^2 = (2\gamma_s)^{-1}$ where $\gamma_s = \overline{E}_s / N_0$. Here $\overline{E}_s$ denotes the average signal energy, and $N_0$ is the single-sided noise spectral density of the additive noise.

For the shadowed Rician channel model, as introduced by Loo [4]–[7], the complex channel gain $\alpha_k$, including log normal LOS term and multipath components, is generated as shown in Fig. 2. Accordingly, $\alpha_k$ is the sum of three components:

$$\alpha_k = A_k + \xi_k + j\eta_k \tag{4}$$

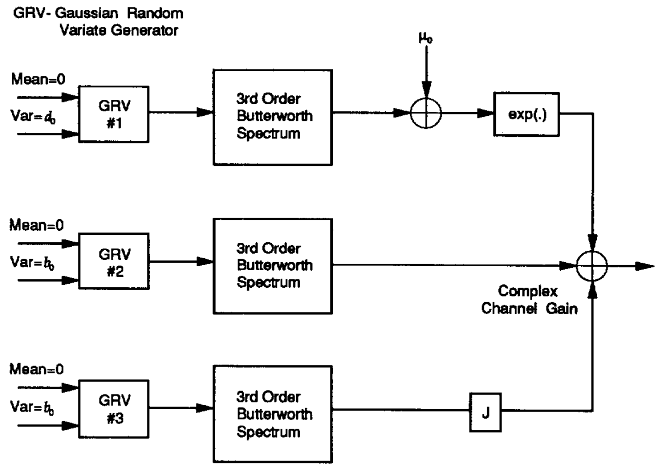


Fig. 2. Shadowed Rician fading simulator.

TABLE I
SHADOWED RICIAN MODEL PARAMETERS

| parameter | Light | Average | Heavy |
|---|---|---|---|
| $b_0$ | 0.158 | 0.126 | 0.0631 |
| $\mu_0$ | 0.115 | -0.115 | -3.91 |
| $\sqrt{d_0}$ | 0.115 | 0.161 | 0.806 |

where both $\xi_k$ and $\eta_k$ are two real independent Gaussian random variables with zero mean and variance $b_0$. The remaining term $A_k$ is equal to exp $(\zeta_k)$ where $\zeta_k$ is Gaussian with mean $\mu_0$ and variance $d_0$ (note that $A_k$ is a constant for nonshadowed Rician fading channels.). The random variables $\xi_k, \eta_k$, and $\zeta_k$ are generated by filtering three independent Gaussian random number sequences. Three identical third-order Butterworth filters of 3-dB cutoff frequency $f_d T_s$ are used for shaping the fading spectrum (see Fig. 2). The measured parameters of this model are given in Table I [8]. Note that the fading is represented by a single sample throughout a symbol interval. This piecewise-constant approximation to the fading process is justified since the fading is slow $(f_d T_s \ll 1)$.

Since $\xi, \eta$, and $\zeta$ have the same fading spectrum, when introducing the autocorrelation function of these, it is convenient to define a wild card # denoting $\xi, \eta$, or $\zeta$. The filter transfer function of a third-order Butterworth filter is [19]

$$|H(f)|^2 = \frac{3}{2\pi f_0} \frac{1}{1+(f/f_0)^6} \tag{5}$$

where $f_0$ is the 3-dB cutoff frequency. Also this spectrum has unit energy gain; that is, the total area under $|H(f)|^2$ is unity. Given the above fading spectrum, the output normalized autocorrelation function is given by [19]

$$\begin{aligned}\rho(\tau) &\triangleq \overline{\#(t)\#(t+\tau)}/\mathrm{var}(\#)\\ &= \frac{1}{2}[\exp(-2\vartheta) + \exp(-\vartheta)(\sqrt{3}\sin(\sqrt{3}\vartheta) + \cos(\sqrt{3}\vartheta))]\end{aligned} \tag{6}$$

where $\vartheta = |\pi f_0 \tau|$. We will later need the normalized correlation coefficient between two adjacent samples:

$$\overline{\#_k \#_{k-1}} = \rho(T_s). \tag{7}$$

As defined in (4), $A_k$ is a lognormally distributed random variable having the probability density function

$$p(x) = \begin{cases} \dfrac{1}{\sqrt{2\pi d_0} x} \exp\left(-\dfrac{(\log(x)-\mu_0)^2}{2d_0}\right), & x > 0 \\ 0, & \text{elsewhere.} \end{cases} \tag{8}$$

It can be readily shown that

$$\overline{|\alpha_k|^2} = \exp(2\mu_0 + 2d_0) + 2b_0, \tag{9}$$

which, for example, is 2.06 dB for the light fading model (Table I). This factor will be included in all signal-to-noise ratio calculations.

For later PEP calculations, we shall first "fix" the additive log normal component of the channel gain $\alpha_k$, obtain the PEP conditional on the sequence of the $A_k$, and then integrate the conditional PEP over the joint pdf of the $A_k$. This approach is justified since the log normal process is assumed to be completely independent of the multipath process.

## IV. THE PEP IN FAST LOG NORMAL FADING

We assume here the availability of some kind of channel measurements; that is, for a sequence of true channel gains $(\alpha_1, \alpha_2, \cdots, \alpha_N)$, there corresponds a sequence of channel estimator [18] outputs denoted as $(\hat{\alpha}_1, \hat{\alpha}_2, \cdots, \hat{\alpha}_N)$. Obviously, the performance of the coded system will be heavily dependent upon the accuracy of these estimates. Depending on the detection technique used, the estimate $\hat{\alpha}_k$ is obtained as follows:

$$\hat{\alpha}_k = \begin{cases} \alpha_k & \text{TC-MPSK} \\ y_{k-1} & \text{TC-MDPSK,} \\ \alpha_k + \zeta_k & \text{TC-MPSK with a pilot} \end{cases} \tag{10}$$

where $\zeta_k$ is an additive noise term, appearing because of the nonzero bandwidth of the pilot tone extraction filter. This will be considered later.

As in [18], we take the Viterbi decoder metric to be Euclidean; namely,

$$m(y_k, x_k) = -|y_k - \beta\hat{\alpha}_k x_k|^2 \tag{11}$$

where $\beta$ is equal to $\mu\sqrt{b_0/b_1}$. Also, the variance of $\hat{\alpha}_k$ is $b_1 = (1/2)\overline{(\hat{\alpha}_k - \overline{\hat{\alpha}}_k)(\hat{\alpha}_k - \overline{\hat{\alpha}}_k)^*}$ where $*$ denotes the complex conjugate. The normalized correlation coefficient between $\hat{\alpha}_k$ and $\alpha_k$ is $\mu = (1/2)\overline{(\alpha_k - \overline{\alpha}_k)(\hat{\alpha}_k - \overline{\hat{\alpha}}_k)*}/\sqrt{b_0 b_1}$. Note also that if perfect channel estimates are available, this decoding metric becomes optimal (in the maximum likelihood sense). Pilot-tone based detection and differential detection approach this ideal performance limit under slow fading and high signal-to-noise ratio conditions.

As we shall see later, the accuracy of the approximations derived herein depends on the value of $\mu$. The closer $\mu$ is to 1, the more accurate are the approximations. This phenomenon is analogous to the behavior of the bit error probability in relation to the accuracy of channel state information. For this reason, we do not consider the absence of channel state information [1], where the channel estimate just consists of phase information and is devoid of amplitude information. In this case, it can be readily shown that the value of $\mu$ is less than 0.9, making our approximation inapplicable.

The PEP $P(\boldsymbol{x} \rightarrow \hat{\boldsymbol{x}})$ is defined to be the probability of choosing the codeword $\hat{\boldsymbol{x}} = (\hat{x}_1, \hat{x}_2, \cdots, \hat{x}_N)$ when $\boldsymbol{x} = (x_1, x_2, \cdots, x_N)$ was transmitted [1], given $\boldsymbol{x}$ and $\hat{\boldsymbol{x}}$ are the only choices. Since only the components of the two codewords that differ contribute to the PEP, assign the set of subscripts $k_i, (i = 1, 2, \cdots, L)$, arranged in ascending order, for which $x_{k_i} \neq \hat{x}_{k_i}$. Note that $L$ is the Hamming distance between $\boldsymbol{x}$ and $\hat{\boldsymbol{x}}$. The smallest possible $L, L_{\min}$, is known as the code *diversity*. The PEP, by using the fact that the total metric for a codeword is the sum of component metrics, is

$$P(\boldsymbol{x} \rightarrow \hat{\boldsymbol{x}}) = \Pr\{\Xi < 0\} \tag{12}$$

where

$$\Xi = \sum_{i=1}^{L} y_{k_i}\beta^*\hat{\alpha}_{k_i}^*(x_{k_i} - \hat{x}_{k_i})^* + y_{k_i}^*\beta\hat{\alpha}_{k_i}(x_{k_i} - \hat{x}_{k_i}). \tag{13}$$

For the PEP in (12), under conditons $\gamma_s \rightarrow \infty$, and $\mu \approx 1$, an approximation has been derived in [15, eq. (30)]. As shown there, for the Rician fading channel we have

$$P(\boldsymbol{x} \rightarrow \hat{\boldsymbol{x}}) \cong B(L)\prod_{i=1}^{L}\frac{\Gamma}{b_0|\mu|^2|x_{k_i} - \hat{x}_{k_i}|^2 + \Gamma} \cdot \exp\left(\frac{A^2\theta|x_{k_i} - \hat{x}_{k_i}|^2}{(b_0|\mu|^2|x_{k_i} - \hat{x}_{k_i}|^2 + \Gamma}\right) \tag{14}$$

where

$$B(L) \cong \frac{1}{\sqrt{2\pi(2L+1)}}, \qquad \Gamma = 4((1 - |\mu|^2)b_0 + \sigma^2) \tag{15}$$

and

$$\theta = \left[-\beta + \frac{2(b_0 + b_1 + \sigma^2)|\beta|^2 - 4\beta|\mu|^2 b_0}{\Gamma}\right]. \tag{16}$$

Although this approximation has been obtained for constant $A_k$, it is also true when $A_k$ varies over the duration of an error event. This assertion holds because the saddle point in this case (see [15, eq. (28)]) is completely independent of the value of $A$. Thus, denoting $\underline{A} = (A_1, A_2, \cdots, A_L)$ the above becomes the conditional pairwise error probability; that is,

$$P(\boldsymbol{x} \rightarrow \hat{\boldsymbol{x}}|\underline{A}) \cong B(L)\prod_{i=1}^{L}\frac{\Gamma}{b_0|\mu|^2|x_{k_i} - \hat{x}_{k_i}|^2 + \Gamma} \cdot \exp\left(\frac{A_i^2\theta|x_{k_i} - \hat{x}_{k_i}|^2}{(b_0|\mu|^2|x_{k_i} - \hat{x}_{k_i}|^2 + \Gamma}\right). \tag{17}$$

Because of ideal interleaving, each $A_i$ is independent. Thus, the pairwise error probability is

$$P(\boldsymbol{x} \rightarrow \hat{\boldsymbol{x}}) \cong B(L)\prod_{i=1}^{L}\int_{-\infty}^{\infty}\frac{\Gamma}{b_0|\mu|^2|x_{k_i} - \hat{x}_{k_i}|^2 + \Gamma} \cdot \exp\left(\frac{A_i^2\theta|x_{k_i} - \hat{x}_{k_i}|^2}{(b_0|\mu|^2|x_{k_i} - \hat{x}_{k_i}|^2 + \Gamma}\right)p(A_i)dA_i \tag{18}$$

where each $p(A_i)$ is given by (8). For light and average shadowed Rician cases (where $d_0$ is small), each of these integrals can be obtained by a method given in [14], where it has been shown that

$$\int_{-\infty}^{\infty} g(t)\exp(-\gamma t^2)dt = \sqrt{\frac{\pi}{\gamma}}\left(g(0) + \frac{1}{4\gamma}g(0)\right) + O(\gamma^{-5/2}), \gamma \rightarrow \infty. \tag{19}$$

Substituting (8) in (18), transforming $t_i = \log A_i - \mu_0$, taking $\gamma = 1/2d_0$, and using (19), the approximate PEP can be expressed as

$$P(\boldsymbol{x} \rightarrow \hat{\boldsymbol{x}}) \cong B(L)\prod_{i=1}^{L}\frac{\Gamma}{b_0|\mu|^2|x_{k_i} - \hat{x}_{k_i}|^2 + \Gamma} \cdot \exp(-c_i\varrho^2)(1 + 2d_0 c_i\varrho^2[c_i\varrho^2 - 1]) \tag{20}$$

where $\varrho = \exp(\mu_0)$ and

$$c_i = \frac{-\theta|x_{k_i} - \hat{x}_{k_i}|^2}{b_0|\mu|^2|x_{k_i}|^2 + \Gamma}. \tag{21}$$

Next we specialize this expression for the three detection methods.

### A. Ideal TC-MPSK

Here, by definition, we have an ideal estimate of the channel gain; that is, $\hat{\alpha}_k = \alpha_k$. Thus, $b_1 = b_0, \mu = 1, \beta = 1$, and $\theta = -0.5$. Substituting these values in (20) leads to the expression

$$P(\boldsymbol{x} \rightarrow \hat{\boldsymbol{x}}) \cong B(L)\prod_{i=1}^{L}\frac{1 + 2d_0 c_i\varrho^2[c_i\varrho^2 - 1]}{1 + \frac{b_0}{2}|x_{k_i} - \hat{x}_{k_i}|^2\gamma_s}\exp(-c_i\varrho^2) \tag{22}$$

where

$$c_i = \frac{\frac{1}{4}|x_{k_i} - \hat{x}_{k_i}|^2\gamma_s}{1 + \frac{b_0}{2}\left|x_{k_i} - \hat{x}_{k_i}|^2\gamma_s\right.}, \tag{23}$$

This expression can be readily used to compute the average bit error probability via the standard transfer function bounding technique.

To assess the accuracy of (22), we compare it with the Chernoff bound for this case. Using [1, eq. (20)] and [14, eq. (9)], it can be readily shown that

$$P(\boldsymbol{x} \rightarrow \hat{\boldsymbol{x}}) \leq \frac{1}{2} \prod_{i=1}^{L} \frac{1}{\sqrt{\pi}} \frac{1}{1 + \frac{b_0}{2}|x_{k_i} - \hat{x}_{k_i}|^2\gamma_s} \psi_1 \tag{24}$$

where

$$\psi_i = \int_{-\infty}^{\infty} \exp \cdot \left( -v^2 - \frac{\frac{1}{4}|x_{k_i} - \hat{x}_{k_i}|^2\gamma_s}{1 + \frac{b_0}{2}|x_{k_i} - \hat{x}_{k_i}|^2\gamma_s} \exp\left(2\sqrt{2d_0}v + 2\mu_o\right) \right) dv. \tag{25}$$

This integration can be solved using the quadrature algorithms. As discussed in [12], a factor of one-half is included in (24).

### B. TC-MDPSK

Here, for any signaling period, the preceding signal provides the channel estimate; that is, $\hat{\alpha}_k = \alpha_{k-1} + n_{k-1}$ (see (2), (3), and (10)). The term $v_{k-1}$ is now absorbed in the channel gain term. Hence, the channel estimate has a variance of $b_1 = b_0 + \sigma^2$ and it follows that

$$|\mu|^2 = \frac{b_0\rho^2(T_s)}{b_0 + 0.5\gamma_s^{-1}} = \frac{b_0\delta}{b_0 + 0.5\gamma_s^{-1}} \tag{26}$$

where $\rho(\cdot)$ is the normalized autocorrelation function for a third-order Butterworth spectrum given by (7), and $\delta \triangleq \rho^2(T_s)$. An examination of (26) reveals two facts. First, for very slow fading (i.e., $\rho(T_s) \approx 1$), at large signal-to-noise ratios $\mu$ approaches unity. Hence, the quality of the channel estimates is ideal. Second, for fast fading ($\rho(T_s) < 1$), no matter how large the signal-to-noise ratio, $\mu$ remains less than unity. This implies, for $\gamma_s \rightarrow \infty$, a fixed error probability, which is usually termed as an "error floor."

Substituting $|\mu|^2$ in (20) results in the expression

$$P(\boldsymbol{x}\rightarrow\hat{\boldsymbol{x}}) \cong B(L) \prod_{i=1}^{L} \cdot \frac{(b_0(1-\delta)\gamma_s + 1 + (4b_0\gamma_s)^{-1})(1 + 2d_0c_i\varrho^2[c_i\varrho^2 - 1])}{\frac{b_0}{4}\delta|x_{k_i} - \hat{x}_{k_i}|^2\gamma_s + b_0(1-\delta)\gamma_s + 1 + (4b_0\gamma_s)^{-1}} \cdot \exp\left(-c_i\varrho^2\right) \tag{27}$$

where

$$c_i = \frac{-0.25\theta|x_{k_i} - \hat{x}_{k_i}|^2\gamma_s(1 + 0.5(b_0\gamma_s)^{-1})}{\frac{b_0}{4}\delta|x_{k_i} - \hat{x}_{k_i}|^2\gamma_s + b_0(1-\delta)\gamma_s + 1 + (4b_0\gamma_s)^{-1}}. \tag{28}$$

As noted in [15], the accuracy of (27) will decrease with the increasing Doppler spread. This is due to the fact that the increased Doppler decreases the value of $\mu$, as shown in (26). For the three shadowing cases, the value of $b_0$ decreases from light to heavy; as a result, the performance of differentially detected TCM degrades, and so does the accuracy of (27). Note also that comparing the PEP for TC-MPSK (22) and that of TC-MDPSK (27) reveals that the latter is inferior by 3 dB.

### C. TC-MPSK with a Pilot Tone

As an alternative to differential detection, the $\alpha_k$ may be measured using some technique such as a pilot tone [18] or embedded pilot symbols [20]. If a reference tone is transmitted along with the data signal (both within the coherence bandwidth of the fading process), and if this tone can be filtered ideally, the resulting system performance will be almost equal to that of ideal coherent detection. Here, we assume these conditions. A further discussion regarding the validity of these assumptions can be found in [21].

For our purpose, we simply need to determine how the pilot-tone estimate correlates with the true channel gain. As in [18], the estimate $\hat{\alpha}_k$ is obtained by a pilot tone extraction filter whose frequency response is

$$H(f) = \begin{cases} \frac{1}{P}, & -B_p/2 \leq f \leq B_p/2 \\ 0, & \text{otherwise} \end{cases} \tag{29}$$

where $P$ is the amplitude of the pilot tone, and $B_p$ is the bandwidth of the pilot tone filter. Now the fraction of the total power spent on the data signal and the pilot tone is $1/(1+r)$ and $r/(1+r)$, respectively, where $r = P^2T_s$. As in [18], we assume $B_p = 2f_d$. Then, the output of this filter is

$$\hat{\alpha}_k = \alpha_k + \frac{\zeta_k}{P} \tag{30}$$

where $\zeta_k$ is a complex Gaussian random variable with zero mean and a variance of $B_pN_0$. It then follows that

$$\begin{aligned} \mathrm{var}(\hat{\alpha}_k) &= b_1 = b_0 + 0.5(B_pT_s)\left(\frac{1+r}{r}\right)\gamma_s^{-1} \\ |\mu|^2 &= \frac{b_)}{b_0 + 0.5(B_pT_s)\left(\frac{1+r}{r}\right)\gamma_s^{-1}} \end{aligned} \tag{31}$$

where $\gamma_s$ now accounts for the total symbol energy spent on both the data and pilot-tone. We note here that as $\overline{E}_s/N_0$ increases, the value of $|\mu|^2$ approaches unity. Thus, at large signal-to-noise ratios, the pilot tone technique is essentially equivalent to ideal coherent detection

By substituting these in (20), we have (32) and (33), which are shown at the bottom of the next page.

## V. The PEP for Slow Log Normal Fading

In the preceding discussion, we assumed that all three components of the channel gain (4) have an equal fading bandwidth. In the following, we assume that the log normal component varies slowly in comparison to the multipath component. Consequently, the log normal variate $A_k$ in (4) will remain constant during short error events. In other words, the interleaving depth is sufficient to break up correlations due to multipath components but not those due to the shadowing component.

As derived for the case of fast fading, the PEP here too is

$$P(\boldsymbol{x} \to \hat{\boldsymbol{x}}) \cong \int_{-\infty}^{\infty} \left[ B(L) \prod_{i=1}^{L} \frac{\Gamma}{b_0|\mu|^2|x_{k_i} - \hat{x}_{k_i}|^2 + \Gamma} \cdot \exp\left( \frac{A^2\theta|x_{k_i} - \hat{x}_{k_i}|^2}{b_0|\mu|^2|x_{k_i} - \hat{x}_{k_i}|^2 + \Gamma} \right) \right] p(A)dA \tag{34}$$

where $p(A)$ is given by (8). This can be evaluated in the same manner as in the case of fast fading. Consequently, we maintain that for the light and average shadowing models the PEP is given by

$$P(\boldsymbol{x} \to \hat{\boldsymbol{x}}) \cong B(L)\left( \frac{\Gamma \exp(-c_i\varrho^2)}{b_0|\mu|^2|x_{k_i} - \hat{x}_{k_i}|^2 + \Gamma} \right) \cdot (1 + 2d_0c_0\varrho^2[c_0\varrho^2 - 1]) \tag{35}$$

where $\varrho$ and $c_i$ are as defined earlier, and

$$c_o = \sum_{i=1}^{L} \frac{-\theta|x_{k-i} - \hat{x}_{k_i}|^2}{b_0|\mu|^2|x_{k_i} - \hat{x}_{k_i}|^2 + \Gamma}. \tag{36}$$

Unfortunately, this expression cannot be used with the transfer function method because $c_0$ consists of additive terms, a manifestation of our slow fading assumption. As in [14], we compute $c_0$ only for the shortest error event, and incorporate this value of $c_0$ into $B(L)$. Thus, for this case

$$B(L) = B_1(L) = \frac{1}{\sqrt{2\pi(2L+1)}} \cdot (1 + 2d_0c_0\varrho^2[c_0\varrho^2 - 1])_{L_{\min}}. \tag{37}$$

As before, we next specialize this expression for the three detection methods.

### A. Ideal TC-MPSK

As discussed earlier, we have an ideal estimate of the channel gain, that is, $\hat{\alpha}_k = \alpha_k$. Thus $b_1 = b_0, \mu = 1, \beta = 1$, and $\theta = -0.5$. Substituting these values in (35) leads to the expression

$$P(\boldsymbol{x} \to \hat{\boldsymbol{x}}) \cong B_1(L) \prod_{i=1}^{L} \frac{\exp(-c_i\varrho^2)}{1 + \frac{b_0}{2}|x_{k_i} - \hat{x}_{k_i}|^2\gamma_s}. \tag{38}$$

Furthermore, the constant $c_0$ is given by

$$c_0 \approx \frac{0.5L_{\min}}{b_0}, \qquad \gamma_s \to \infty \tag{39}$$

which is independent of the distance structure of the shortest error event. Thus, $B_1(L)$ depends only on the length of the shortest error event.

### B. TC-MDPSK

By following the discussion in Section III B, we have the PEP for a slow log normal fading case:

$$P(\boldsymbol{x} \to \hat{\boldsymbol{x}}) \cong B_1(L) \prod_{i=1}^{L} \cdot \frac{(b_0(1-\delta)\gamma_s + 1 + (4b_0\gamma_s)^{-1}) \exp(-c_i\varrho^2)}{\frac{b_0}{4}\delta|x_{k_i} - \hat{x}_{k_i}|^2\gamma_s + b_0(1-\delta)\gamma_s + 1 + (4b_0\gamma_s)^{-1}}. \tag{40}$$

### C. TC-MPSK with a Pilot Tone

Substituting the correlation coefficient and variance (31) of the pilot-tone based estimate in (35), we have (41), which is hown at the bottom of the next page.

$$P(\boldsymbol{x} \to \hat{\boldsymbol{x}}) \cong B(L) \prod_{i=1}^{L} \cdot \frac{\left[\frac{B_pT_s(1+r)}{r} + 1 + r\right] + \frac{B_pT_s(1+r)^2}{2b_0r}\gamma_s^{-1}}{\frac{b_0}{2}|x_{k_i} - \hat{x}_{k_i}|^2\gamma_s + \left[\frac{B_pT_s(1+r)}{r} + 1 + r\right] + \frac{B_pT_s(1+r)^2}{2b_0r}\gamma_s^{-1}} \times \exp(-c_i\varrho^2)(1 + 2d_0c_i\varrho^2[c_i\varrho^2 - 1]) \tag{32}$$

where

$$c_i = \frac{-0.5\theta|x_{k_i} - \hat{x}_{k_i}|^2\gamma_s\left(1 + \frac{B_pT_s(1+r)^2}{2b_0r}\gamma_s^{-1}\right)}{\frac{b_0}{2}|x_{k_i} - \hat{x}_{k_i}|^2\gamma_s + \left[\frac{B_pT_s(1+r)}{r} + 1 + r\right] + \frac{B_pT_s(1+r)^2}{2b_0r}\gamma_s^{-1}}. \tag{33}$$

## VI. Phase Jitter Analysis

In [8], [9], the authors computed the standard deviation of the absolute and differential phases of the true channel gain. This section derives their pdf's for fast fading, shadowed Rician channel. Specifically, denoting the $k$th channel gain as $V_k e^{j\phi k}$, we determine the pdf of $\phi_k$ and $(\phi_k - \phi_{k-1})$.

### A. Absolute Phase

Taking the channel gain $\alpha_k$ in (4), we drop the subscript $k$ for notational convenience, and convert $\alpha$ into form $Ve^{j\phi}$. Thus, after some elementary manipulations, the conditional joint pdf of the envelope $V$ and the phase $\phi$ can be obtained as

$$p(V, \phi | A) = \frac{V}{2\pi b_0} \exp\left(\frac{A^2 - 2AV\cos\phi + V^2}{2b_0}\right) \quad (42)$$

where $0 \leq V < \infty$ and $0 \leq \phi \leq 2\pi$. To find the joint pdf of $(V, \phi)$, (42) must be averaged over the pdf of $A$. Thus, from (42) and (8) we have

$$p(V, \phi) = \frac{V}{2\pi b_0} \frac{1}{\sqrt{2\pi d_o}} \int_{-\infty}^{\infty} \cdot \exp -\left(\frac{\varrho^2 e^{2t} - 2\varrho e^t V\cos\phi + V^2}{2b_0}\right) \cdot \exp -\left(\frac{t^2}{2d_0}\right) dt \quad (43)$$

where $\varrho = \exp \mu_0$, as defined earlier. Since for light and average shadowing cases $d_0$ is quite small, an approximate expression for this integral can be obtained as before. Using only the first term of the expansion given in (19), we have

$$p(V, \phi) = \frac{V}{2\pi b_0} \exp -\left(\frac{\varrho^2 - 2\varrho V\cos\phi + V^2}{2b_0}\right) + O(d_0^{3/2}). \quad (44)$$

Integrating this over the variable $V$ results in

$$p(\phi) \cong \frac{\varrho\cos\phi}{\sqrt{2\pi b_0}} \exp -\left(\frac{\varrho^2 \sin^2\phi}{2b_0}\right). \quad (45)$$

Clearly, for small values ($\cos\phi \approx 1, \sin\phi \approx \phi$), $\phi$ is Gaussian with zero mean and variance $b_0/\varrho^2$. For a light fading channel, this turns out to be a standard deviation of 20.3 degrees, which agrees quite well with the computed value 22.7 degrees [9]. As observed in [19], the phase process of a Rician fading process is approximately Gaussian with zero mean and variance $1/(2K)$. It thus follows that the equivalent $K$ factor of a shadowed channel is $\varrho^2/2b_0$.

TABLE II
Differential Phase Standard Deviation in Degrees

| Bandwidth | Light | Average |
|---|---|---|
| 0.025 | 2.3 | 2.7 |
| 0.05 | 4.4 | 5.1 |
| 0.1 | 8.1 | 9.3 |
| 0.2 | 14.3 | 16.0 |

Similarly, concerning the envelope process, note that integrating (44) over the phase $\phi$ yields

$$p(V) \approx \frac{V}{b_0} \exp -\left(\frac{\varrho^2 + V^2}{2b_0}\right) I_0\left(\frac{\varrho V}{b_0}\right) \quad (46)$$

where $I_0(\cdot)$ is the zero-order modified Bessel function. Since this expression is the pdf of a Rician fading amplitude (see [1]), it is possible to define a $K$ factor, as in a Rician channel. Here $K = \varrho^2/2b_0$, as also obtained above. For light and average fading models this turns out to be 6 and 5 dB, respectively. A similar observation is made in [10], [14].

In light of the foregoing, we conclude that, on a first-order basis, the light and average shadowing channels are Rician. However, if the second order terms are included, this equivalence breaks down.

### B. Differential Phase

Since differential phase statistics depend on the correlation between two temporally adjacent channel gains, and since two correlated log normal variates are also involved, this case is a lot more complicated than that of absolute phase. Note, however, that interleaving does not affect this correlation (differential detection exploits the intrinsic channel memory) and that interleaving is sufficient to make $(\phi_k - \phi_{k-1})$ terms independent of each other, as we have assumed at the beginning.

In view of this difficulty, we can only provide an approximate pdf that must be computed numerically. In the appendix, it is shown that the differential phase $\varphi$ is distributed approximately as

$$p(\varphi) = \int_0^{2\pi} p(\phi_1, \phi_1 + \varphi) d\phi_1, \qquad \text{for } -\pi \leq \varphi \leq \pi. \quad (47)$$

Computed values of the standard deviation of differential phase in degrees are shown in Table II, and they agree quite well with the values given in [8].

$$P(\boldsymbol{x} \rightarrow \hat{\boldsymbol{x}}) \cong B_1(L) \prod_{i=1}^{L} \cdot \frac{\left(\left[\frac{B_p T_s(1+r)}{r} + 1 + r\right] + \frac{B_p T_s(1+r)^2}{2b_0 r}\gamma_s^{-1}\right) \exp(-c_i \varrho^2)}{\frac{b_0}{2}|x_{k_i} - \hat{x}_{k_i}|^2 \gamma_s + \left[\frac{B_p T_s(1+r)}{r} + 1 + r\right] + \frac{B_p T_s(1+r)^2}{2b_0 r}\gamma_s^{-1}}. \quad (41)$$

## VII. Error Performance of TCM Schemes

This section presents a comparison between Monte-Carlo simulation results and the approximations we developed in the previous sections.

### *A. The Union Bound on the Average Bit Error Probability*

Typically, the average bit error probability of a communication system is one of the most important performance measures. A tight upper bound on this measure can be obtained via the union bound, which consists of infinitely many terms. Based on the PEP expressions developed here, all the terms may be enumerated using a transfer function. Then, the bit error probability of a TCM scheme with ideal interleaving/deinterleaving is bounded as

$$P_b \leq \frac{B(L_{\min}}{n} \frac{\partial T(D_1, D_2, \cdots, I)}{\partial I}\bigg|_{I=1} \tag{48}$$

where $n$ is the number of input bits per encoding interval, and the $D_i$ are the product terms in the approximations derived before, excluding $B(L)$, with each $D_i$ being associated with $|x_{k_i} - \hat{x}_{k_i}|^2$. Note that the number of distinct $D_i$ is finite and that $B(L_{\min}$ is included because $B(L)$ is a decreasing function of $L$. The transfer function $T(D_1, D_2, \cdots, I)$ is determined by a signal flow graph, using *weight profile* and *uniformity* property [22].

In this study, we use a rate 2/3, eight-state binary convolutional encoder (see Fig. 3) to confirm the accuracy of the approximations developed thus far. The reader is referred to [12] for more details regarding the derivation of modified state transition diagram, augmented branch labels, and the modified encoder transfer function for this code.

### *B. Computer Simulations*

The rate 2/3 8-state convolutional encoder with 8-PSK signal set was used to encode a random data stream (the code is taken from (12)]. The receiver was implemented using a Viterbi alogrithm, with the decoding metric given in (11). In the Viterbi decoder, a decision depth of 18 symbols was used, that is, 6 times the code memory [9]. Although our theoretical results were derived under the assumption of ideal interleaving, the simulation was carried out using a finite interleaving depth. For a fading bandwidth of 0.05, the interleaving depth was set to 10 symbols. This choice gives an effective bandwidth of 0.5, at which the correlation between any two adjacent, deinterleaved symbols becomes negligible. This effect can be verified from (7), where a zero of $\rho(T_s)$ is found near 1 when $f_0 = 0.5$.

In the case of pilot-tone based detection, about 30% of the transmitted power was allocated to the pilot-tone, which is optimum [15], [18] for the fading bandwidth considered herein.

When simulating the slow fading log normal component, the bandwidth of the low-pass filter of that component (see Fig. 2) was set to 0.001. After interleaving, the effective log normal fade rate would still be 0.01, which is slow enough that the log normal component remains roughly constant for several adjacent symbol intervals (as assumed in Section IV).

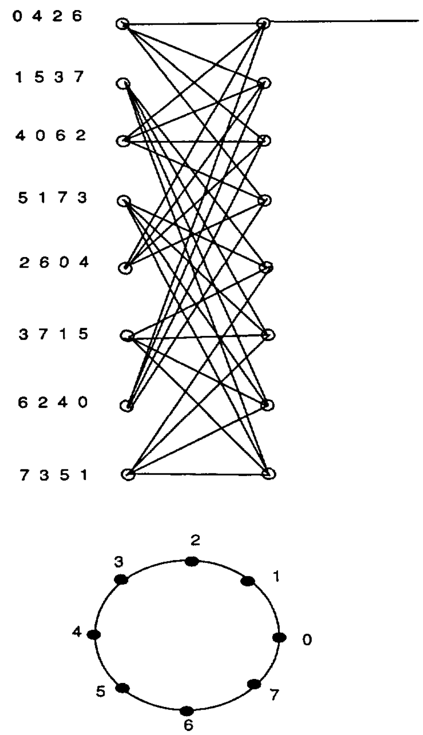


Fig. 3. Trellis diagram for 8-state, 8 PSK TCM scheme [12].

To reduce the uncertainty of each simulation point, as in [23], each point was simulated at least twice: first with a given number of error events, second with twice that number. This was repeated until the two results were within 10% of each other. For $P_b \geq 10^{-4}$ the starting number of error events was 200, while for $P_b < 10^{-4}$ the number was 100. For these two ranges of $P_b$, the accuracy of the estimates varies from 20% to 30% with a confidence level of 95%.

For light and average cases, and for coherent, differential and pilot-tone based detection methods, we present $P_b$ versus $\overline{E}_b/N_0$ performance in Figs. 4–9. For both coherent and pilot-tone methods, the bounds are quite tight when $P_b \leq 10^{-3}$. As noticeable from these figures, the error bounds fare better in the average shadowed channel than in the light shadowed channel. The reason is that the variance of multipath component $b_0$ is smaller for the former. As can be seen from [15, eq. (27)], smaller $b_0$ improves the saddlepoint approximation presented therein.

For differential detection, however, the error bounds are looser, as can be seen in Figs. 5, 8. Here the error bounds will improve with decreasing Doppler. The results presented are for a 5% Doppler rate, which can be considered as a worst case for the 800 MHz frequency band. Another reason for not considering Doppler rates above that figure is that pulse distortion and intersymbol interference effects introduced by fading can no longer be neglected.

The slow log normal fading case is treated in Figs. 10–12. Once again, there is satisfactory agreement between error bounds and simulation results.

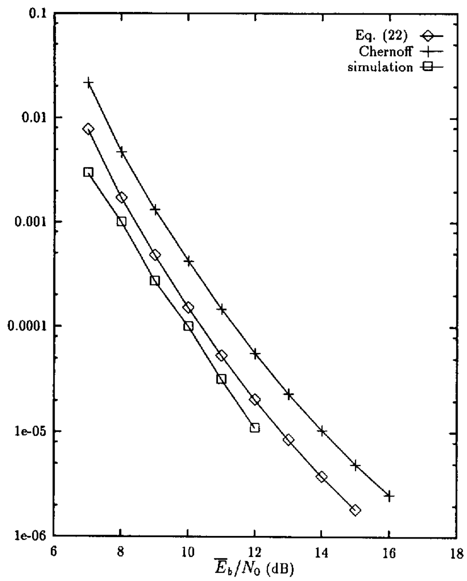


Fig. 4. $P_b$ versus $\overline{E}_b/N_0$. Trellis code in Fig. 3, light shadowed Rician fading, coherent detection.

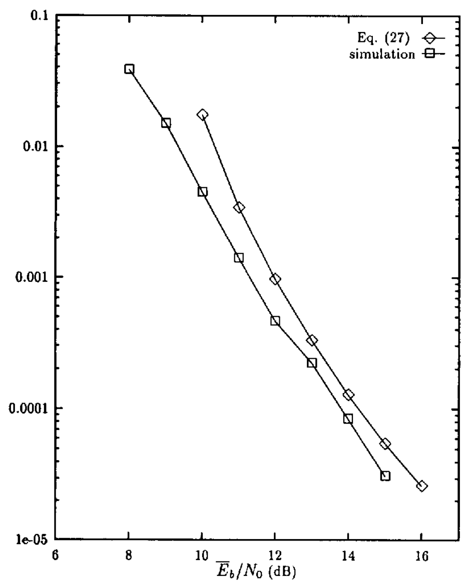


Fig. 5. $P_b$ versus $\overline{E}_b/N_0$. Trellis code in Fig. 3, light shadowed Rician fading, differential detection, $f_dT_s = 0.05$.

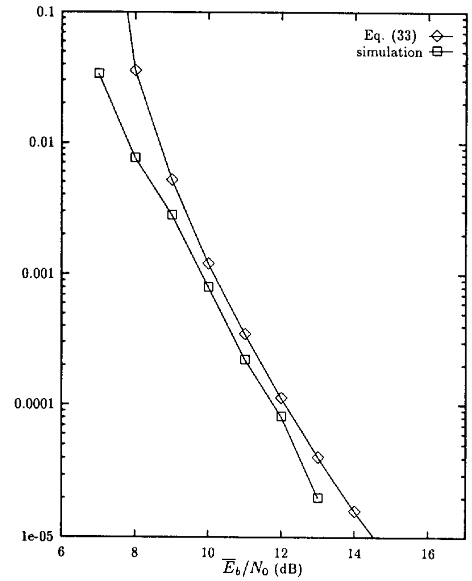


Fig. 6. $P_b$ versus $\overline{E}_b/N_0$. Trellis code in Fig. 3, light shadowed Rician fading, pilot-tone detection, $f_dT_s = 0.05$.

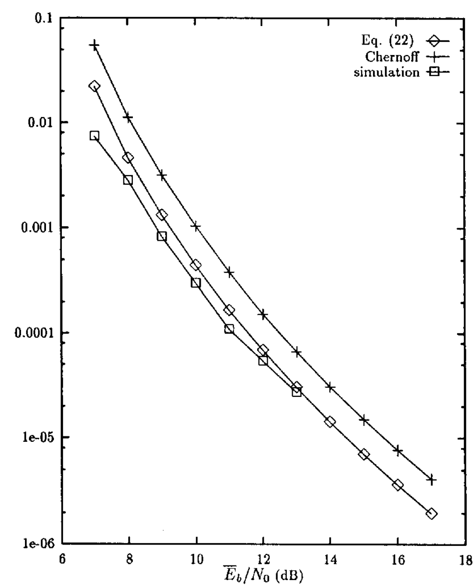


Fig. 7. $P_b$ versus $\overline{E}_b/N_0$. Trellis code in Fig. 3, average shadowed Rician fading, coherent detection.

## VIII. Conclusions

New approximations for the PEP of TCM schemes operating on the shadowed Rician fading channel have been derived, which can be readily used with the transfer function method to obtain an upper bound on the bit error probability. The application of the resulting bounds has been exemplified for a moderately complex eight-state TCM scheme transmitted through this channel. For bit error rates less than $1 \times 10^{-3}$, the derived error bounds for coherent and pilot-tone detections are within a fraction of a dB of the simulation results. For differential detection the difference is larger, though, assuming a worst-case Doppler fading bandwidth of 0.05. It is felt that the results will be useful in evaluating the performance of TCM schemes over shadowed channels, and that the analysis enhances the understanding of this channel model.

## IX. Appendix

Without any loss of generality, let us write $\alpha_k = \alpha_1$ and $\alpha_{k-1} = \alpha_2$. From the channel gain in (4), if follows that

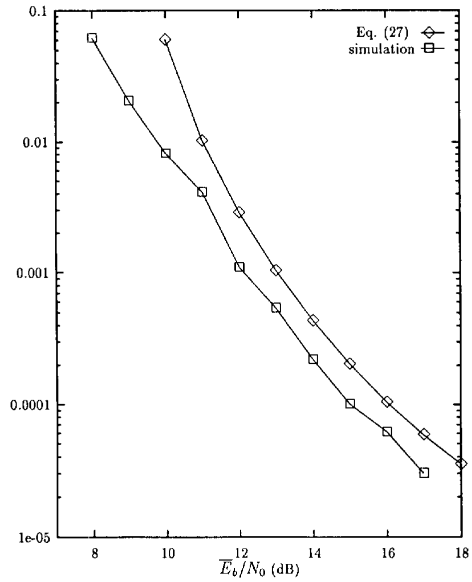


Fig. 8. $P_b$ versus $\overline{E}_b/N_0$. Trellis code in Fig. 3, average shadowed Rician fading, differential detection, $f_dT_s = 0.05$.

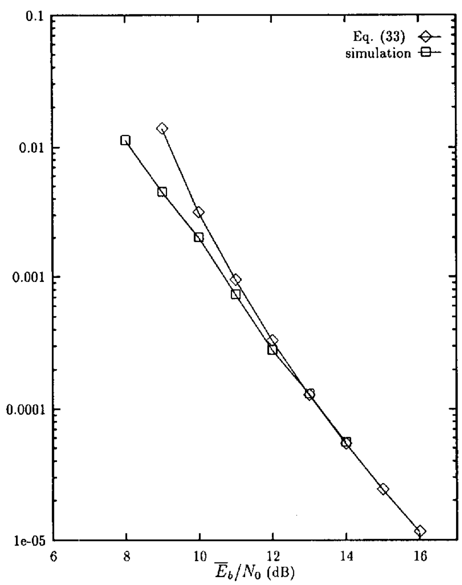


Fig. 9. $P_b$ versus $\overline{E}_b/N_0$. Trellis code in Fig. 3, average shadowed Rician fading pilot-tone detection, $f_dT_s = 0.05$.

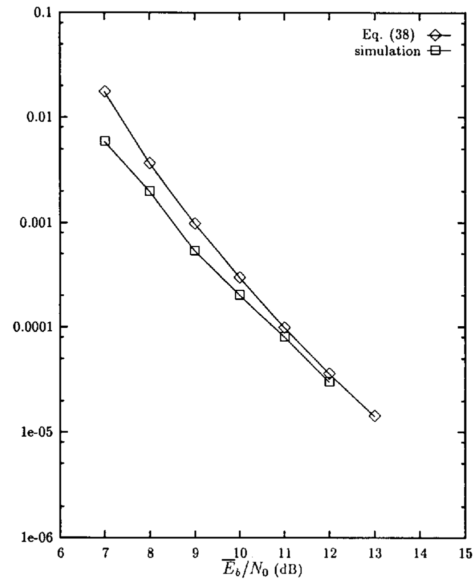


Fig. 10. $P_b$ versus $\overline{E}_b/N_0$. Trellis code in Fig. 3, light shadowed Rician slow fading, coherent detection.

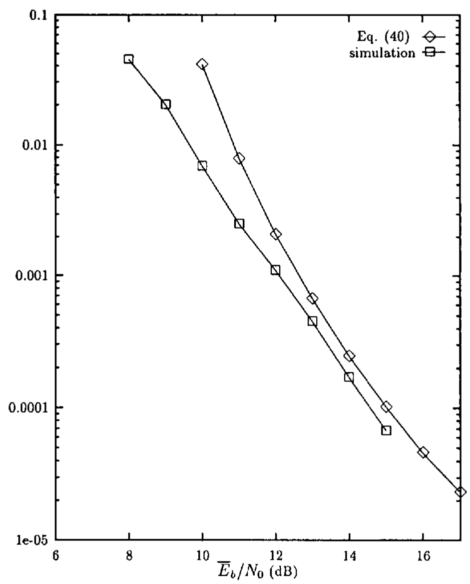


Fig. 11. $P_b$ versus $\overline{E}_b/N_0$. Trellis code in Fig. 3, light shadowed Rician slow fading, differential detection, $f_dT_s = 0.05$.

the pairs $\xi_1, \xi_2$ and $\eta_1, \eta_2$ are identically and independently distributed. Thus, their joint pdf is

$$p(\xi_1, \xi_2, \eta_1, \eta_2) = \kappa \exp \cdot \left(-\frac{1}{2\sigma_1^2}(\xi_1^2 + \xi_2^2 - 2\rho\xi_1\xi_2 + \eta_1^2 + \eta_2^2 - 2\rho_1\eta_1\eta_2)\right) \quad (49)$$

where $\rho_1 = \rho(T_s), \sigma_1^2 = b_0(1 - \rho_1^2), \kappa = 1/(4\pi^2 b_0^2(1 - \rho_1^2))$.

Let us also introduce the following transformations: $r_1 \cos\phi_1 = e^{\zeta_1 + \mu_0} + \xi_1, r_1 \sin\phi_1 = \eta_1, r_2 \cos\phi_2 = e^{\zeta_2 + \mu_0} + \xi_2, r_2 \sin\phi_2 = \eta_2$. Now it is a simple matter to show that

$$p(r_1, \phi_1, r_2, \phi_2 | \zeta_1, \zeta_2) = \kappa r_1 r_2 \exp\left(-\frac{1}{2\sigma_1^2}\Delta_0\right) \quad (50)$$

where

$$\Delta_0 = \varrho^2(e^{2\zeta_1} + e^{2\zeta_2} - 2\rho_1 e^{\zeta_1+\zeta_2}) - 2r_1\varrho\cos\phi_1(e^{\zeta_1} - \rho_1 e^{\zeta_2}) \cdot -2r_2\varrho\cos\phi_2(e^{\zeta_2} - \rho_1 e^{\zeta_1}) - 2\rho_1\cos\varphi r_1 r_2 + r_1^2 + r_2^2 \quad (51)$$

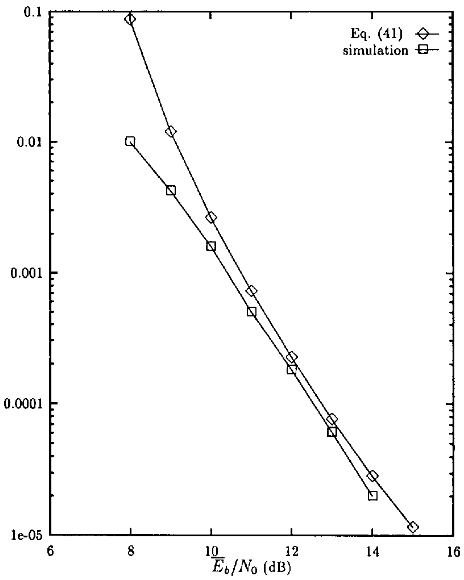


Fig. 12. $P_b$ versus $\overline{E}_b/N_0$. Trellis code in Fig. 3, light shadowed Rician, slow fading, pilot-tone detection, $f_dT_s = 0.05$.

where $\varphi = \phi_1 - \phi_2$ is the differential phase in which we are interested. To derive (50), we have made use of the fact that $A_k$ in (4) is a log normal variable. Moreover, according to the shadowed Rician model, $\zeta_1$ and $\zeta_2$ are jointly distributed as

$$p(\zeta_1, \zeta_2) = \frac{1}{2\pi d_0\sqrt{1-\rho_1^2}} \cdot \exp\left(-\frac{1}{2d_0(1-\rho_1^2)}(\zeta_1^2 + \zeta_2^2 - 2\rho_1\zeta_1\zeta_2)\right). \quad (52)$$

Once again, we note that the term $1/2(2d_0(1-\rho_1^2))$ will be quite large for both light and average shadowed fading cases. Therefore, an approximate expansion for the average of (50) with respect to (52) can be obtained via Laplace's method in two dimensions. In [24, 8.2] it is shown that an integral of the form

$$I(\lambda) = \int_{\mathcal{D}} \exp\{\lambda\,\phi(\boldsymbol{x})\}g_0(\boldsymbol{x})d\boldsymbol{x}, \qquad \boldsymbol{x} = (x_1, x_2) \quad (53)$$

can be approximated as

$$I(\lambda) \approx \frac{2\pi}{\lambda}\frac{g_0(\boldsymbol{x}_0)\exp\{\phi(\boldsymbol{x}_0)\}}{(\phi_{x_1x_1}(\boldsymbol{x}_0)\phi_{x_2x_2}(\boldsymbol{x}_0) - \phi_{x_1x_2}^2(\boldsymbol{x}_0))^{1/2}}, \quad \text{as } \lambda \to \infty \quad (54)$$

where $\boldsymbol{x}_0$ is an interior critical point of $\phi(\boldsymbol{x})$.

The critical point of our function (52) is (0, 0). Thus, we conclude from (54) that

$$p(r_1, \phi_1, r_2, \phi_2) \approx \kappa r_1 r_2 \exp\left(-\frac{1}{2\sigma_1^2}\Delta_1\right) \quad (55)$$

where

$$\Delta_1 = 2\varrho^2(1-\rho_1) - 2r_1\varrho\cos\phi_1(1-\rho_1) - 2r_2\varrho\cos\phi_2(1-\rho_1) - 2\rho_1\cos\varphi r_1r_2 + r_1^2 + r_2^2. \quad (56)$$

We can convert this into the sum of a bivariate quadratic of $r_1$ and $r_2$ and an expression of $\phi_1$ and $\phi_2$, thereby enabling the integration of (55) over $r_1$ and $r_2$. We then have

$$p(\phi_1, \phi_2) \approx \kappa_1 \cdot \left(\frac{b_0(1-\rho_1^2)\rho_1\cos\varphi}{(1-\rho_1^2\cos^2\varphi)^{1.5}} + \frac{\varrho^2(1-\rho_1)^2}{(1-\rho_1^2\cos^2\varphi)^{2.5}}\Delta_2\right) \cdot \exp\frac{-\varrho^2}{2b_0(1+\rho_1)}\Delta_3 \quad (57)$$

where $\kappa_1 = 1/(2\pi b_0)$,

$$\Delta_2 = (\rho_1\cos\varphi\cos^2\phi_1 + (1+\rho_1^2\cos^2\varphi) \cdot \cos\phi_1\cos\phi_2 + \rho_1\cos\varphi\cos^2\phi_2) \quad (58)$$

and

$$\Delta_3 = 2 - \frac{1-\rho_1}{1-\rho_1^2\cos^2\varphi} \cdot (\cos^2\phi_1 + 2\rho_1\cos\varphi\cos\phi_1\cos\phi_2 + \cos^2\phi_2). \quad (59)$$

Our aim is to find the pdf of $\varphi = \phi_1 - \phi_2$. As defined, $\varphi$ can vary from $-2\pi$ to $2\pi$; however, it is desirable to confine $\varphi$ from $-\pi$ to $\pi$. To do this we use a method given in [25, 1.5.4]. Thus, we finally have

$$p(\varphi) = \int_0^{2\pi} p(\phi_1, \varphi + \phi_1)d\phi_1, \qquad -\pi \le \varphi \le \pi. \quad (60)$$

## References


[1] D. Divsalar and M. K. Simon, "Trellis-coded modulation for 4800 to 9600 bps transmission over a fading satellite channel," *IEEE J. Select. Areas Commun.*, vol. 5, pp. 162–175, Feb. 1987.

[2] M. K. Simon and D. Divsalar, "The performance of trellis-coded multilevel DPSK on a fading mobile satellite channel," *IEEE Trans. Veh. Technol.*, vol. 37, pp. 78–91, Feb. 1988.

[3] D. Divsalar and M. K. Simon, "The design of trellis coded MPSK for fading channels: Set partitioning for optimum code design," *IEEE Trans. Commun.*, vol. 36, pp. 1013–1021, Sept. 1988.

[4] C. Loo, "A statistical model for a land mobile satellite link," *IEEE Trans. Veh. Technol.*, vol. 34, pp. 122–127, Aug. 1985.

[5] C. Loo *et al.*, "Measurements and modelling of land-mobile satellite signal statics," in *1986 Vehicular Technology Conf.*, vol. 34, Dallas, TX, May 1986, pp. 262–267.

[6] C. Loo, "A statistical model for a land mobile satellite link," in *Links for the Future* (ICC'84), *Science, Systems and Services for Communication*, P. Dewilde and C. A. May, Eds. New York: IEEE/Elsevier Science Publishers, North Holland, 1984.

[7] C. Loo, "Measurements and models of a mobile satellite link with applications," in *Proc. GLOBECOM'85*, New Orleans, LA, Dec. 1985, pp. 1177–1180.

[8] P. J. McLane *et al.*, "PSK and DPSK trellis codes for fast fading, shadowed mobile satellite communication channels," *IEEE Trans. Commun.*, vol. 36, pp. 1242–1246, Nov. 1988.

[9] P. J. McLane *et al.*, PSK and DPSK trellis codes for fast fading, shadowed mobile satellite communication channels," in *Proc. 1987 Int. Conf. Commun.*, Seattle, WA, June 1988, pp. 726–731.

[10] A. C. M. Lee, "Analysis of amplitude, phase and error distributions for shadowed mobile satellite communication channels," Dep. Elec. Eng., Queen's Univ., Kingston, Ont., Canada, Master's thesis, Aug. 1988.

[11] A. C. M. Lee and P. J. McLane, "Convolutionaly interleaved PSK and DPSK trellis code for shadowed, fast fading mobile satellite communication channels," *IEEE Trans. Veh. Technol.*, vol. 39, pp. 37–47, June 1990.

[12] R. G. McKay *et al.*, "Error bounds for trellis-coded MPSK on a fading mobile satellite channel," *IEEE Trans. Commun.*, vol. 39, pp. 1750–1761, Dec. 1991.

[13] C. Loo and N. Secord, "Computer models for fading channels with applications to digital transmission," *IEEE Trans. Veh. Technol.*, vol. 40, pp. 700–707, Nov. 1991.
[14] J. Huang and L. Campbell, "Trellis coded MDPSK in correlated and shadowed Rician fading channels," *IEEE Trans. Veh. Technol.*, vol. 40, pp. 786–797, Nov. 1991.
[15] C. Tellambura, Q. Wang, and V. K. Bhargava, "A performance analysis of trellis-coded modulation schemes over Rician fading channels," *IEEE Trans. Veh. Technol.*, to be published.
[16] C. W. Helstrom, "Computing the performance of optical receivers with avalanche diode detectors," *IEEE Trans. Commun.*, vol. 36, pp. 61–66, Jan. 1988.
[17] C. W. Helstrom, "Approximate evaluation of detection probabilities in radar and optical communications," *IEEE Trans. Aerosp. Electron. Syst.*, vol. 14, pp. 630–640, July 1978.
[18] J. K. Cavers and P. Ho, "Analysis of the error performance of trellis coded modulations in Rayleigh fading channels," *IEEE Trans. Commun.*, vol. 40, pp. 74–83, Jan. 1992.
[19] S. Y. Mui and J. W. Modestino, "Performance of DPSK with convolutional encoding on time-varying fading channels," *IEEE Trans. Commun.*, vol. 25, pp. 1075–1083, Oct. 1977.
[20] J. K. Cavers, "An analysis of pilot symbol assisted modulation for Rayleigh fading channels," *IEEE Trans. Veh. Technol.*, vol. 40, pp. 686–693, Nov. 1991.
[21] J. K. Cavers, "Performance of tone caliberation with frequency offset and imperfect pilot filter," *IEEE Trans. Veh. Technol.*, vol. 40, pp. 426–434, May 1991.
[22] E. Biglieri and P. J. McLane, "Uniform distance and error probability properties of TCM schemes," *IEEE Trans. Commun.*, vol. 39, pp. 41–52, Jan. 1991.
[23] R. Kerr, "Coherent detection of interleaved CPFSK on various shadowed mobile satellite channels," Dep. Elec. Eng., Queen's Univ., Kingston, Ont., Canada, Master's thesis, Aug. 1989.
[24] N. Bleistein and R. A. Handelsman, *Asymptotic Expansions of Integrals.* New York: Dover, 1986.
[25] W. C. Jakes (Ed.) *Microwave Mobile Communications.* New York: Wiley, 1974.

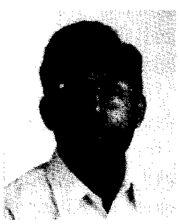

**Chinthananda Tellambura** was born in Anuradhapura, Sri-Lanka, on September 16, 1962. He received the B.Sc. degree in electronics and communications engineering from the University of Moratuwa, Sri-Lanka, in 1986, the M.Sc. degree in electronics from the King's College, University of London, United Kingdom, in 1988, and the Ph.D. degree in electrical engineering from the University of Victoria, Canada, in 1993.

From 1986 to 1987 and 1988 to 1989, he was an Assistant Lecturer at the Department of Electronic Engineering, University of Moratuwa. Presently, he is working as a postdoctoral fellow at the University of Victoria, B.C., Canada. His current research interests include error control coding theory and mobile communications.

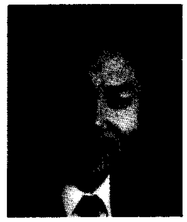

**Qiang Wang** was born in Beijing, China, in June 1961. He received the B.Sc. and M.Sc. degrees from the Nanjing Communications Engineering Institute, Nanjing, China, in 1982 and 1985, respectively, and the Ph.D. degree from the University of Victoria, B.C., Canada, in 1988, all in electrical engineering.

From 1987 to 1990, he was a Member of Technical Staff of Microtel Pacific Research (now MPR Teltech), Ltd., Burnaby, B.C., Canada. He was involved in designs and implementation of various error correction coding and modulation schemes and spread spectrum systems using DSP and VLSI technology. Since March 1990, he has been an Assistant Professor in the Department of Electrical and Computer Engineering at the University of Victoria while being a consultant to MPR and several other companies. His current research interests include spread spectrum communications, error control coding, and personal wireless communications.

**Vijay K. Bhargava** (F'92) received the B.Sc. (Hons.) degree from the University of Rajasthan in 1966, and B.Sc. degree in mathematics and engineering, and the M.Sc. and Ph.D. degrees, both in electrical engineering, from Queen's University in Kingston, Ont., Canada, in 1970, 1972, and 1974, respectively.

After brief stays at the Indian Institute of Science and the University of Waterloo, he joined Concordia University in Montreal and was promoted to Professor in 1984. From 1982 to 1983 he was on sabbatical leave at Ecole Polytechnique de Montreal. In August 1984 he joined the newly formed Faculty of Engineering at the University of Victoria as a Professor of Electrical Engineering. In 1988 he was appointed a Fellow of the BC Advanced Systems Institute. He is a coauthor of the book *Digital Communications by Satellite* (Wiley, 1981). A Japanese translation of the book was published in 1984, while a Chinese translation was published in 1987. During 1988–1990 he served as the Editor of the *Canadian Journal of Electrical and Computer Engineering*. In 1992 he became the Director of IEEE Region 7 for a two-year term.

Dr. Bhargava is a recipient of the IEEE Centennial Medal, the EIC Centennial Medal, and the 1987 A. F. Bulgin Premium awarded by the Institute of Radio and Electronic Engineers (UK). In 1988 he was elected a Fellow of the Engineering Institute of Canada. In 1990 he received the John B. Stirling Medal of EIC.